Revista de Metalurgia
April–June 2018, 54 (2), e120
ISSN-L: 0034-8570
https://doi.org/10.3989/revmetalm.120

Influence of the roughening method, joint configuration and adhesive thickness on the shear strength of ferritic stainless steel surfaces joined by methyl methacrylate

Celso E. Cruz-González[a], José D. Mosquera-Artamonov[b,✉], Saúl D. Santillán[c], Hugo Gámez-Cuatzin[a]

[a]Centro de Ingeniería y Desarrollo Industrial Estado de México, Av. Desarrollo s/n, Parque Industrial Cuamatla, 54763 Cuautitlán Izcalli, México
[b]Posgrado en Ingeniería de Sistemas. Facultad de ingeniería Mecánica y Eléctrica, Universidad Autónoma de Nuevo León, Pedro de Alba s/n, Ciudad Universitaria, San Nicolás de los Garza, N.L., México
[c]Centro de Alta Tecnología, Universidad Autónoma Nacional de México, campus Juriquilla, Av. Playa Pie de la Cuesta No. 702, Desarrollo San Pablo, 76125 Santiago de Querétaro, QRO, México
✉Corresponding author: xoce15@ingenieros.com

Submitted: 6 March 2017; Accepted: 17 December 2017; Available On-line: 5 June 2018

ABSTRACT: Surface roughening, joint configuration, and adhesive thickness were selected as factors to analyze, by using a 2^3 design of experiments, the adhesive joint of AISI 430 steel using Methyl Methacrylate. Scanning electron microscopy observations, roughness-contour measurement and wettability analysis were performed on the adherents to analyze the adhesion, roughness, surface contour and shear strength on the adhesion tests. The statistical analysis yields that the most significant variable was the surface finishing for an adjusted R^2 of 90%. The difference of shear stress of 20.69 and 12.67 MPa was obtained for the mechanical and chemical roughening respectively, since the difference in wettability was around 78 and 113° for the same surface finishing. According to analyze the combination of factors for a shear stress of 21.80 MPa are mechanical roughening, single lap joint and glass beads.

KEYWORDS: Design of experiments; Joint configuration; Methyl methacrylate; Shear strength; Surface roughening

Citation/Citar como: Cruz-González, C.E.; Mosquera-Artamonov, J.D.; Santillán, S.D.; Gámez-Cuatzin, H. (2018). "Influence of the roughening method, joint configuration and adhesive thickness on the shear strength of ferritic stainless steel surfaces joined by methyl methacrylate". *Rev. Metal.* 54(2): e120. https://doi.org/10.3989/revmetalm.120

RESUMEN. *Influencia del método de rugosidad, configuración de la junta y espesor del adhesivo sobre la resistencia al corte de superficies de acero inoxidable ferrítico unidas por metacrilato de metilo.* Las variables rugosidad superficial, configuración de la junta y espesor de adhesivo fueron seleccionadas para analizarlas mediante un diseño de experimentos 2^3. La unión adhesiva se realizó en una junta de acero ASI 430 utilizando Metil metacrilato como adhesivo. Para analizar la adhesión, rugosidad, contorno superficial y resistencia al corte se realizaron observaciones en el Microscopio Electrónico de Barrido, mediciones de rugosidad-contorno y mediciones de humectabilidad sobre los adherendos. El análisis estadístico arrojó que la variable más significativa fue el acabado superficial generando una R^2 de 90%. Una diferencia de 20,69 y 12,67 MPa se obtuvo para los acabados superficiales mecánico y químico debido a una diferencia en humectabilidad expresada por ángulos de contacto de 78 y 113° respectivamente. Con base al diagrama de Pareto, la combinación para obtener el esfuerzo de 21,80 MPa fue el acabado mecánico, junta de bisel simple y perlas de vidrio.

PALABRAS CLAVE: Configuración de juntas; Diseño de experimentos; Metacrilato de metilo; Resistencia a la cizalladura; Rugosidad superficial

ORCID ID: Celso E. Cruz-González (https://orcid.org/0000-0001-7620-9052); José D. Mosquera-Artamonov (https://orcid.org/0000-0001-5419-6561); Saúl D. Santillán (https://orcid.org/0000-0003-2556-1640); Hugo Gámez-Cuatzin (https://orcid.org/0000-0003-3402-4476)

1. INTRODUCTION

Adhesive bonding, mechanical fastening, and welding, are technologies typically used to join metallic parts during a product assembly (Bermejo *et al.*, 2008; Cruz *et al*., 2014). In traditional fusion welding process, work-pieces are joined by the application of an external heat source that melts the base material around the interface producing welding beads and heat affected zones. The using of high temperatures might affect the quality, accuracy and reliability of the joined parts, modifying most of the times, the mechanical performance of the welding (Mori *et al.*, 2013). In addition, during the welding process of ferritic stainless steel, the heat source produces an adverse effect in its mechanical properties (elongation, stress, corrosion resistance and energy) due to an incipient grain growth (AWS, 2007).

Nowadays, classical fusion welding (arc and spot), are the industrial dominating methods to join metals. Although the using of these welding techniques is widespread, they present some disadvantages; for instance, spot resistance welding and arc welding produce weld marks on the welded surface and cannot be used for outer body-panel joining. A similar phenomenon occurs with welding of ferritic stainless steel, since its difference in carbon content could affect ductility and toughness. Recently, a comparative study of fillet welds was performed on plates of AISI 430 and DIN 1.4003 ferritic grade steels (6 mm thick). Results suggested that the high carbon content of AISI 430 promotes sensitization, martensitic formation on the grain boundary, a reduction of 50% in toughness, 15% in elongation and 30% increase in Vickers in hardness mainly in the heat affected zone.

Since these welding methods are often restricted to low-carbon steels, a different approach to join other materials; such as high-carbon steels, high strength steels, and aluminum alloys are needed. In this sense, adhesive bonding (as disruptive technology), is gaining interest in the automotive industry due to its versatility to join metals, composite materials and other dissimilar materials. Proper application of adhesive joining can improve corrosion resistance, increase the fatigue strength, damps vibration, provides smooth contour, among other benefits (Kreibich and Marcantonio, 1987; Bergström and Brottare, 1996; Ebnesajjad and Landrock, 2015a). In this context, Karachalios *et al.* (2013) have investigated, for one and two components epoxy resins, the effect of overlapping length and adherent thickness for high and low strength steels. They observed that for a high strength adherent and a short overlap, the failure is dominated by adhesive global yield. In contrast, for large overlap the failure occurs by local shear strains and adherent yielding.

On the other hand, substrate surface preparation is probably one of the most important steps in the adhesion process, since it makes the adherent surface receptive to the development of strong and durable adhesive joints. It is desirable, although not always practical; to have the adherent directly exposed to the adhesive, without an oxide film, paint, primer, chromate coating or silicone release agents. These layers, could act as a weak boundary material blocking the adhesive contact to the adherent surface (Ebnesajjad and Landrock, 2015b). For these reasons, selection of the surface preparation method depends on the adherent type, size of component parts, and the rapid depletion of active chemicals in the immersion bath (or accumulation of foreign materials in the bath) might improve the adhesion.

The above suggest that the combination of surface finishing method and adhesive formulation must be analyzed to determine the influence of the surface preparation and adhesive on a specific adherent. An alternative to analyze the effect of the surface preparation method on the shear strength of ferritic stainless steel joined by methyl methacrylate is the design of experiments (DOE) methodology. DOE is frequently used to describe, or explain, the variation of information, under different variables, that have a strong effect on the response (Cruz-González *et al.*, 2016). DOE not only involves the selection of suitable predictors and responses, but planning the delivery of the experiment under statistically optimal conditions given the constraints of available resources (machines, apparatus for quality control, etc).

Use of DOE on adhesive joining is limited in the actual literature, only a few studies have been reported for different manufacturing processes. For instance; Jin and Shi (2000) proposed a new methodology based on design of experiments to make prognosis of feature extraction from stamping tonnage signal considering variable interactions. Feng and Kusiak (2000) used the

design of experiments for concurrent selection of component tolerances and the corresponding manufacturing processes trying to minimize the variation of tolerance stackups. The DOE approach was applied by Lanzotti *et al.* (2015), to understand Process Parameter Effects of RepRap Open-Source Three-Dimensional Printers due a significant lack of scientific data on the performance of open-source 3D systems and on the selection of adequate process parameters that can help to improve the quality of the parts. DOE also was applied by Cruz *et al.* (2014). To improve the welding parameters to obtain an optimal Charpy impact test upon a mechanized GTAW process for welding 6Al4V titanium alloy. Brient *et al.* (2011), used the technique to study the influence of grinding parameters on glass work-pieces surface finish.

In the present work is analyzed, by using a design of experiments, the influence of surface finishing (mechanical and chemical roughness), joint configuration (single and beveled), and thickness (the use or not of glass beads) on the shear strength. Methyl Methacrylate MP55420 adhesive, a two component adhesive specifically engineered for structural bonding of thermoplastics, metal substrates, composite materials, and dissimilar materials (Ahesive Systems Inc., 2017), was selected as adhesive. The substrates were AISI 430 ferritic steels sheets. Lap Shear tests were carried out to obtain the joint shear strength. For analytical purposes, wettability testing and surface contour were performed to obtain information of the surface finishing effect (mechanical and chemical roughening). Finally scanning electron microscopy was used to study the surface finishing and thus obtain qualitative information to compare each one. To the best of the author's knowledge, there are not enough scientific papers containing a structured and detailed description of the ferritic stainless steels adhesion process (by using methyl methacrylate) and its statistical analysis, by using design of experiments.

2. MATERIALS AND METHODS

2.1. Adherents and adhesive

AISI 430 of 200×120×1.2 mm sheets (tensile strength of 530 MPa, 0.2% yield strength of 330 MPa and 38% of elongation at 50 mm of gage length), were employed as adherents. The selected adhesive was a commercial MP55420 Methyl Methacrylate, manufactured by ASI®, with and without glass beads. These glass beads (0.150 mm of diameter, 47 HRC, 69 MPa of compressive strength and a chemical composition of 70–100% of silicon-sodium-calcium glass) could produce a thickness around 0.150 mm. For the adhesive application on the adherent surface, gun nozzles manufactured by Adhesives Systems INC were employed.

Table 1. Factors and levels for the selected 2^3 design of experiments

Factor/Levels	-1	1
A: Surface finishing	Chemical roughening	Mechanical roughening
B: Joint configuration	Beveled lap joint	Single lap joint
C:Adhesive thickness	Without glass beads (0.33 mm thickness)	With glass beads (0.130 mm thickness)

2.2. Design of experiments

A factorial experimental design (FED) type 2^3 was followed to test the single lap shear (SLS) of the bonded stainless steel sheets. This method evolves two levels: low (−1) and high (+1) and three factors: surface finishing method (A), joint configuration (B), and adhesive thickness control method (C), see Table 1. The selection of this factional design allows one to work with eight samples (plus one additional measure).

The running of the experimental tests was defined by using Minitab® software. The analysis of variance (ANOVA) was used to identify, whether or not, the process variable that has a significant effect on the selected responses due to different variable setups. A Pareto chart was performed to show the graphical influence of the variables upon the response (shear strength).

2.3. Coupons surface finishing

According to the FED, two set of four stainless steel sheets were prepared by mechanical and chemically roughing ASTM D2651-01 (2001). The mechanical roughening was carried out by hand sanding with an 80 graded sand paper. The surface finishing was made taking care in preventing deep gouges formation (which are not conducive to good bonding). Finally, the specimens were rinsed with acetone and dried with forced air at 50 °C.

The chemical roughening, was made by immersing the test specimens in a 3500 ml beaker with acid etch (hydrochloric, sulfuric-dichromate) for 10 min at 60 to 65 °C. The acid etch mix, had the following solution (by weight): 45 parts water, 50 parts hydrochloric acid (sp. gr 1.2), 10 parts formalin solution (40%), to 2 parts hydrogen peroxide (concentration, 30 to 35%). After the chemical etch, the specimens were rinsed (with distilled water) and immersed in sulfuric acid-dichromate solution for 5 min (50 to 65 °C). Finally, the specimens were rinsed with distilled water, then with acetone and dried with forced air at 50 °C.

The coupons (25.4×120×1.2 mm) were cut by a mechanical shearing press from Okamoto, fulfilling

the tolerances addressed in ASTM D1002-10 (2010). Later on, coupons were bonded by pressing the adhesive cartridge with the gun to pass through the nozzle. At this point, the resin and the activator get mixed to a ratio 2:1. The adhesive was extended on the surface wetting it. Before bonding, approximately 25 mm in length of adhesive was applied on a side dummy steel sheet to assure that the optimal mixture of adhesive was applied. Afterwards, a uniform pressure of 0.15 MPa was applied to put in intimate contact both adherent surfaces. To keep uniform pressure, a Lap Shear fixture designed by the authors, was used until the handling time was reached.

The handling time for the adhesive was around 10 min until the exothermic reaction was finished. Then, the full curing occurred 20 min after the adhesive reached the room temperature (Adhesive Systems Inc., 2017). After full curing was reached, the test specimens were storage for 24 h on a desiccator; this time obeys an empirical rule of the adhesive manufacturer which recommends this cycle to reach the strength properties. After the cycle was completed the lap shear test were carried out.

2.4. Surface finishing characterization

2.4.1. Wettability testing

A Goniometer model VCA Optima of AST Products Inc., was used following the procedures stated in ASTM D7334-8 (2013). For all measurements, a 5 mL of deionized water droplet was dispersed on the chemically and mechanically roughened surfaces. According to the standard, six measurements were diagonally. Water was used for the testing by following the procedures stated on previous works (Kubiak, *et al.*, 2009; Pappas *et al.*, 2009; Kubiak *et al.*, 2011a; Kubiak *et al.*, 2011b; Dyamenahalli *et al.*, 2015).

2.4.2. Profilometry measurements

In order to obtain a 3D surface profiles a 1-cm^2 sample of the AISI 430 steel sheet was mounted on a Bruker Profilometer with white light at VSI mode and 20x objective. Profilometry was carried out on the specimen following a zig zag path and six lectures were taken. The tridimensional surface pattern was mapped out with Gwydion® Software. The image analysis from the Gwydion® software yielded the roughness pattern on a 3D picture and a graphical configuration for contour and roughness.

2.4.3. Scanning Electron Microscopy (SEM) observations

A JEOL JSM 6610-LV scanning electron microscope was used to observe both, mechanical and chemical roughening surface finishing on a sample of 1x1cm. The work distance was 10 mm, 15 kV of energy applied though filament and secondary electron image were employed.

2.4.4. Post fracture analysis

In this analysis, visual inspection, optical microscopy and scanning electron microscopy were carried out in order to obtain information related to the failure of the most representative specimens that, in this case, were the ones who yield the higher and the lower shear strength.

2.5. SLS tests

SLS test were performed in order to know the shear strength, obtained from the different conditions summarized in the Table 1. After the test coupons were prepared (according to Section 2.3), knurled wedge grips were employed to hold the test specimen on an Instron 4482 Electromechanical Testing Machine. Tabs of 31.10×25.40×1.20 mm, made of AISI 430 were bonded with MP55420 (adhesive bond-line thickness ≈ 0.10 mm) on both sides of every test specimen to ensure the application of axial loading. The speed of testing was of 1.3 mm·min^{-1}. The shear strength was calculated by dividing the maximum applied load then divided by the shear area. Figure 1 depicts a scheme of test specimen dimensions.

3. RESULTS

3.1. Surface analysis

3.1.1. Surface morphology observations

Figure 2 displays the surface finishing of the coupons prior to the adhesive bonding process. Figure 2a shows a low magnification SEM micrograph corresponding to a chemical roughened sample. The surface morphology reveals a uniformly distributed linear pattern with some deep lines that

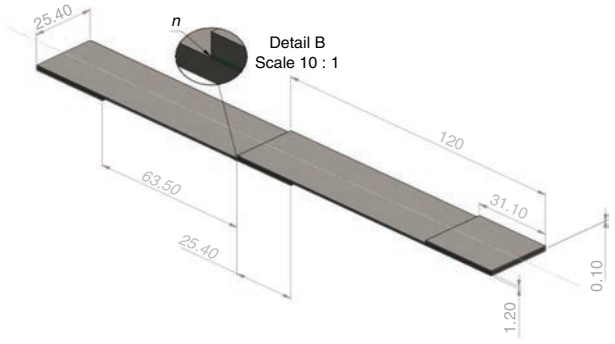

FIGURE 1. Test specimen scheme for the Lap Shear Test (according to the ASTM D1002-10 (2010)).

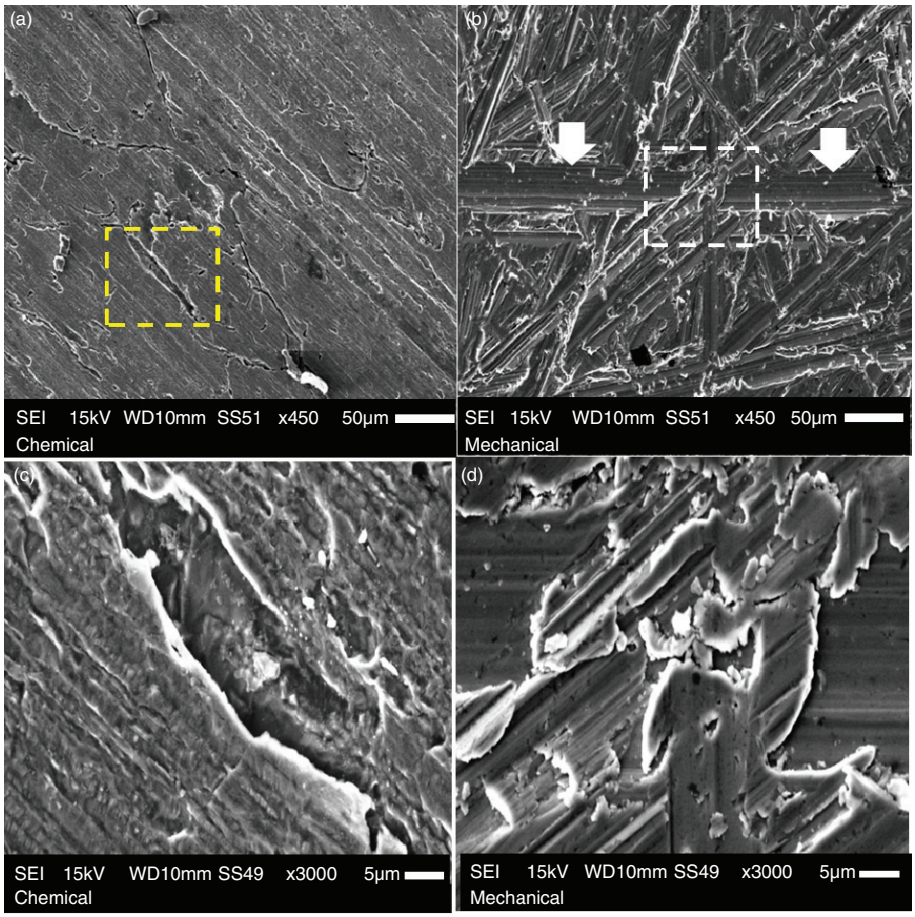

FIGURE 2. SEM micrographs of the surface for: a) chemical roughen, b) mechanical roughening; c) and d) are a zoom of the rectangle zone of each micrograph.

can be observed in detail on the micrograph of Fig. 2b, obtained at higher magnification. Figure 2c also shows a low magnification SEM micrograph but corresponds to a mechanical roughened coupon. Here, a randomized linear pattern is observed. Figure 2d shows an enlarger view of the surface (from the squared area in Fig. 2c) revealing the presence of micro burrs. These observations provide a visual guide of the difference obtained from the mechanical roughening processes; since important differences in the textures and the width and depth of the patterns are identified on the these surfaces.

The latter is explained by the differences of the roughening process, as the chemical process was carried out in a bath and the chemical action was applied uniformly upon the surface, unlike the mechanical roughening in which a manual process was employed yielding differences in pressure and line distribution influenced by the operator.

3.1.2. Surface roughness and contour

Profilometry analyses provided a tridimensional image, in which the surface finishing profile and waviness can be detected. Figure 3 is a 3D profile acquired on the test coupons previous to bonding. A qualitative analysis of the difference between the chemical and mechanical surface finishing treatments can be obtained from this profile comparison.

Figure 3a is the tridimensional profilometry image from the coupon chemically treated. Here, the highest peak has a height ≈ 13 µm; Fig. 3b also is a profilometry image but corresponds to a mechanically roughed coupon. Here, the highest peak has a height ≈ 8.2 µm. pointing out at the qualitative differences between the surface finishing methods, Fig. 3a shows that the chemical roughening actually consists of peaks and valleys evenly distributed throughout the surface. These peaks and valleys are higher and deeper than initially thought from the SEM inspections. On the other hand, mechanical roughening induces randomized marks with different depth and width, as observed in the region located between the arrows in Fig. 3b. These observations are in agreement with the morphology previously described in the SEM micrographs of Fig. 2b and Fig. 2d.

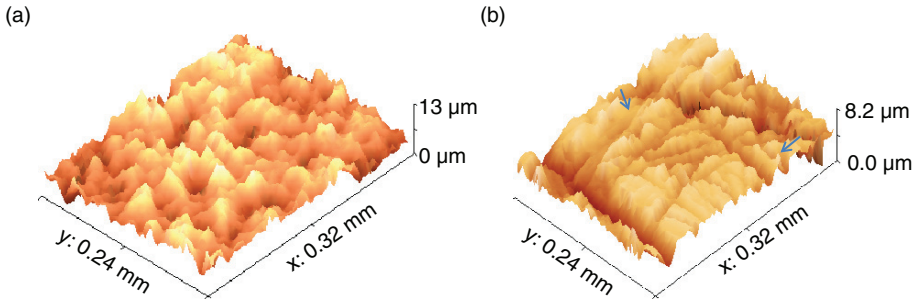

FIGURE 3. Profilometry surface analysis for: a) chemical and b) mechanical roughening.

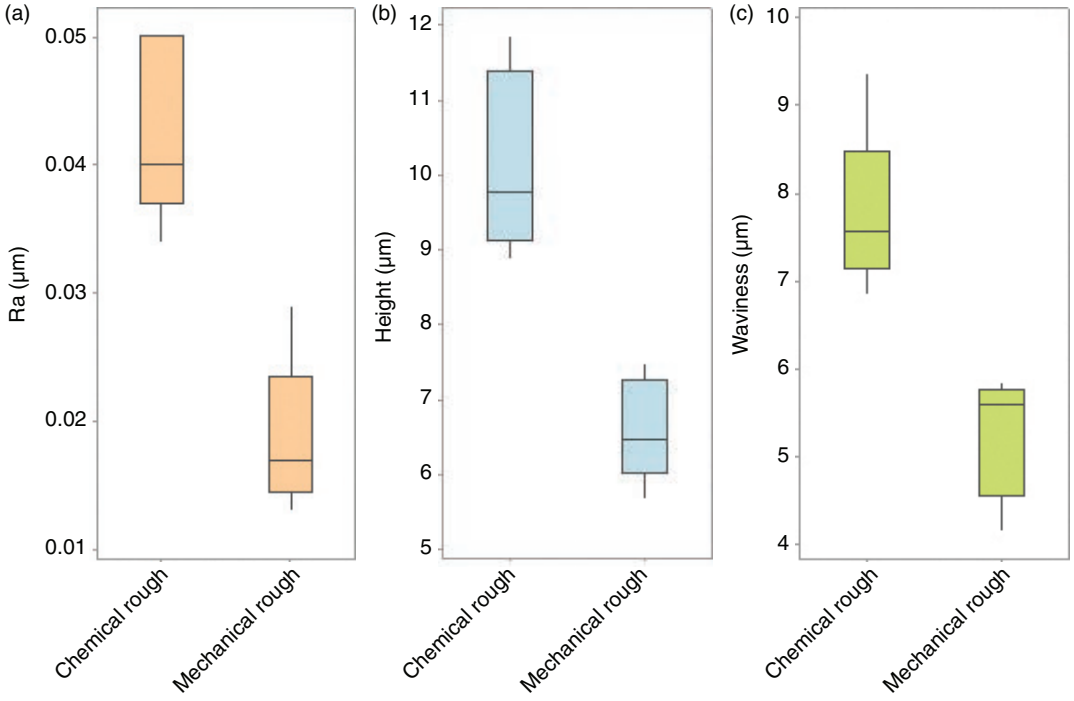

FIGURE 4. Graphical comparison between: a) R_a, b) P_t and W_a; for both surface finishing.

Figure 4 depicts the average results of the average roughness (R_a), the maximum height profile (P_t), and maximum waviness (w_a), obtained from the profilometry measurements. According to Fig. 4a, R_a from the chemical roughening method is higher in comparison to the mechanical one, but the mechanical roughening surface finishing has 22% more scattering that the chemical roughening process. Figure 4b is a bar chart with error bars that shows the average results of the P_t for both surface finishing (mechanical and chemical roughening); in this case the chemical roughening has higher height profiles in comparison of the chemical process; also the chemical roughening process scattering is about 35% higher than the mechanical one. Finally, Fig. 4c depicts the average results for w_a where chemical roughening process has the highest waviness and scattering (20% more in the chemical process).

Figure 5 is a detailed analysis performed to the waviness of the coupons. In the waviness of Fig. 5a, the highest peak is ≈ 17.77 mm, the lowest valley is ≈ 10.26 mm, and the highest distance between peaks is ≈ 72.77 mm. In contrast, Fig. 8b depicts the waviness for the mechanical roughening process, where the highest peak is ≈ 11 mm and the lowest valley ≈ 6.18 mm. The highest distance between peaks is ≈ 33.66 mm. The difference of the peak to valley is 6.76 mm for the chemical roughening process and 4.75 mm for the mechanical roughening one. These results suggests that the chemical roughen sample has larger cavities in comparison to the mechanically roughened one.

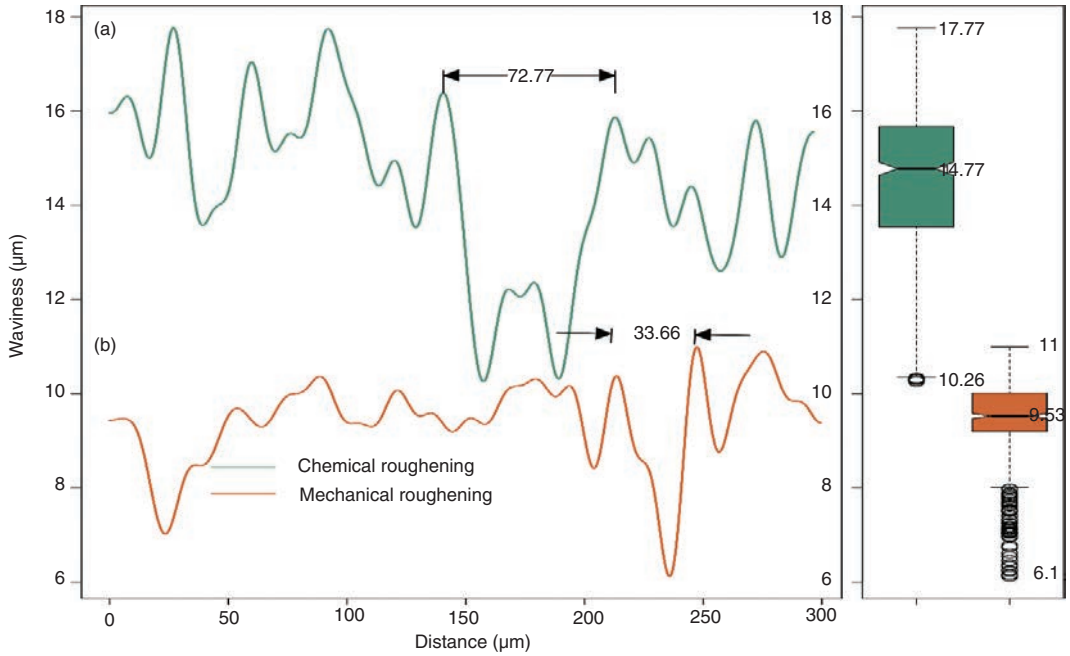

FIGURE 5. a) Chemical and b) mechanical roughening waviness; c) represents a box diagram of the average and the maximum-minimum values as error bars.

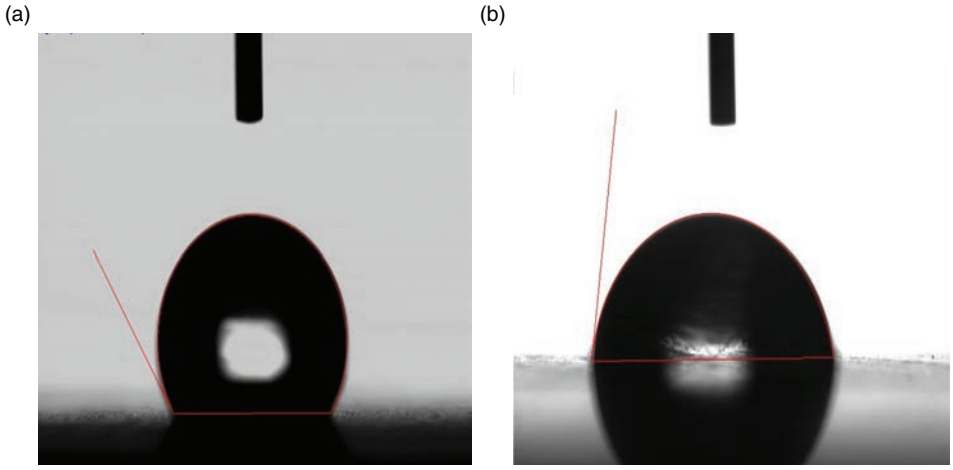

FIGURE 6. Wettability test over the surface finishing for; a) chemical roughening and b) mechanical roughening.

Figure 5c is a box diagram, with error bars, that represents the chemical and mechanical roughening waviness and their statistical variability. As can be noted the average waviness for the chemical roughening method is 14.77 mm. Here, there are just a few outlier values are around 10.19 mm (near of its lowest limit value of 10.26 mm). This is a result of the abrupt pattern found across the surface. On the contrary, the mechanical roughening process has an average waviness value of 9.53 mm and present more outlier values ranging from values of 6.1 to 8 mm. This obviously occurs, since deeper valleys are uncommon for this surface finishing.

3.1.3. Contact angle measurement

Figure 6 shows the effect of the surface roughening in the contact angles, Fig. 6a shows the wettability test carried out on the chemical roughen surface. Observe that the water droplet is not extended enough on this surface; since the drop has a circular shape, Fig. 6b is the wettability test carried out

on the mechanical roughen surface. Here the droplet yields a semicircular shape indicating a higher degree of wetting.

The average experimental contact angle for chemical roughened sample is 113.2 ± 6.2°; whereas for the mechanical roughened is 77.3 ± 4.7°. Commonly, contact angles higher than 90° are considered as having poor wetting. In contrast, contact angles smaller than 90° are considered as having good wetting (Shanahan and Possart, 2011). In this sense, results suggest that the wettability is better in the mechanical roughening than for the chemical process.

3.1.4. Shear Strength statistical analyses

The experimental matrix and combination of factors, obtained from the DOE, are summarized in the Table 2. Results suggest that the run number 4 (mechanical surface roughening, single joint configuration and without glass beads), presents the highest shear strength (20.60 MPa). On the other hand, run number 11 (chemical roughening process, a bevel lap joint and without glass beads), yielded a shear strength value of 12.39 MPa.

The analysis of variance (ANOVA) showed in Table 3, presents an adjusted correlation coefficient (R^2) of 99.26% and P values smaller than 0.05 for factors A and B, and the following combination of factors: AB, AC, BC and ABC; indicating that all of them are statistically significant; therefore, the prediction model can be adjusted to a linear equation. Additionally, the analysis of residuals, according to Kolmogorov-Smirnov test, indicates that theses behave according to a normal distribution (as P value is bigger than 0.05).

Figure 7 shows a Pareto Chart to highlight the most important factor, among a typical large set of factors, on the shear strength; in this case, the surface finishing, the joint configuration, the adhesive thickness control and, they interactions. Accordingly to the chart, the surface finishing is the factor that has the highest influence on the shear strength; on the contrary, the thickness control presents the lowest influence on the shear strength (see in Fig. 7 that $C < 2.31$).

For the contact angle measurements, a similar trend could be observed, since the P value for these measurements tends to be zero. The main effect plot depicted on the Fig. 8, shows that the mean result for the contact angle is strongly affected for the surface finishing, since the slope between the mechanical and chemical-roughening methods is the highest. Although, the influence of the surface finishing was clearly pointed out on Fig. 7, the Fig. 8 illustrates how the numerical value has a priority upon the result of this experiment.

3.1.5. Visual inspection and post fracture analysis

Figure 9 shows the optical images, acquired with a photographic camera, for samples obtained from runs 11 and 4. Here, is detected a significant difference in the fracture features, between the samples.

TABLE 2. Results of the experiment in terms of shear strength

Randomized Runs	Surface Roughening	Joint Configuration	Adhesive Thickness Control	Shear Strength (MPa)	Contact angle (°)
4	Mechanical	Single	without glass beads	20.60	71
7	Chemical	Single	with glass beads	18.62	113
6	Mechanical	Bevel	with glass beads	18.03	73
11	Chemical	Single	without glass beads	12.39	116
9	Chemical	Bevel	without glass beads	16.68	116
8	Mechanical	Single	with glass beads	19.40	69
1	Chemical	Bevel	without glass beads	16.48	113
3	Chemical	Single	without glass beads	12.55	114
10	Mechanical	Bevel	without glass beads	18.83	73
15	Chemical	Single	with glass beads	18.77	116
16	Mechanical	Single	with glass beads	19.10	65
14	Mechanical	Bevel	with glass beads	18.12	78
13	Chemical	Bevel	with glass beads	12.67	121
12	Mechanical	Single	without glass beads	20.29	72
5	Chemical	Bevel	with glass beads	13.48	120
2	Mechanical	Bevel	without glass beads	18.96	78

TABLE 3. Results of the analysis of variance for shear strength results

Source of Variations	Freedom degrees	Adjusted sum of squares	Adjusted mean square	F Value	P Value
Model	7	120.755	17.251	288.930	0.000
Linear	3	67.374	22.458	376.140	0.000
A:Surface Finishing	1	62.766	62.766	1051.250	0.000
B:Joint Configuration	1	4.484	4.484	75.100	0.000
C:Adhesive thickness control	1	0.124	0.124	2.080	0.187
2-Way Interactions	3	27.853	9.284	155.500	0.000
AB: Surface Finishing* Joint Configuration	1	0.369	0.369	6.180	0.038
AC: Surface Finishing* Adhesive thickness control	1	5.605	5.606	93.880	0.000
BC: Joint Configuration* Adhesive thickness control	1	21.879	21.879	366.440	0.000
3-Way Interactions	1	25.528	25.528	427.560	0.000
ABC: Surface Finishing* Joint Configuration* Adhesive thickness control	1	25.528	25.528	427.560	0.000
Error	8	0.478	0.060		
Total	15	121.233			
R-sq. 99.61%			R.-sq (ajust) 99.26%		

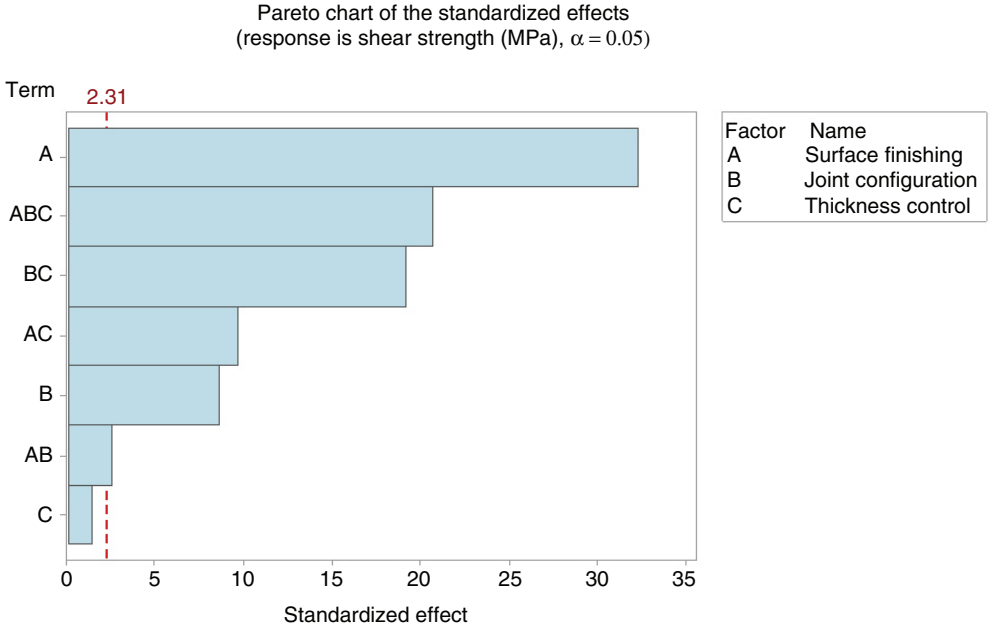

FIGURE 7. Pareto chart for the variables studied in the experimental surface finishing.

Sample 11 seems to have rougher fracture morphology than sample 4 suggesting that the adhesive fracture mode is bigger in sample 11, since this specimen shows a fracture tending to cohesive mode (Ebnesajjad and Landrock, 2015a). The observed zones indicated by the red and green arrows on Fig. 9 (specimen number 11) and yellow and green arrows (specimen number 4).

Figure 10 presents SEM micrographs obtained for samples number 4 and 11, Fig. 10a is a micrograph

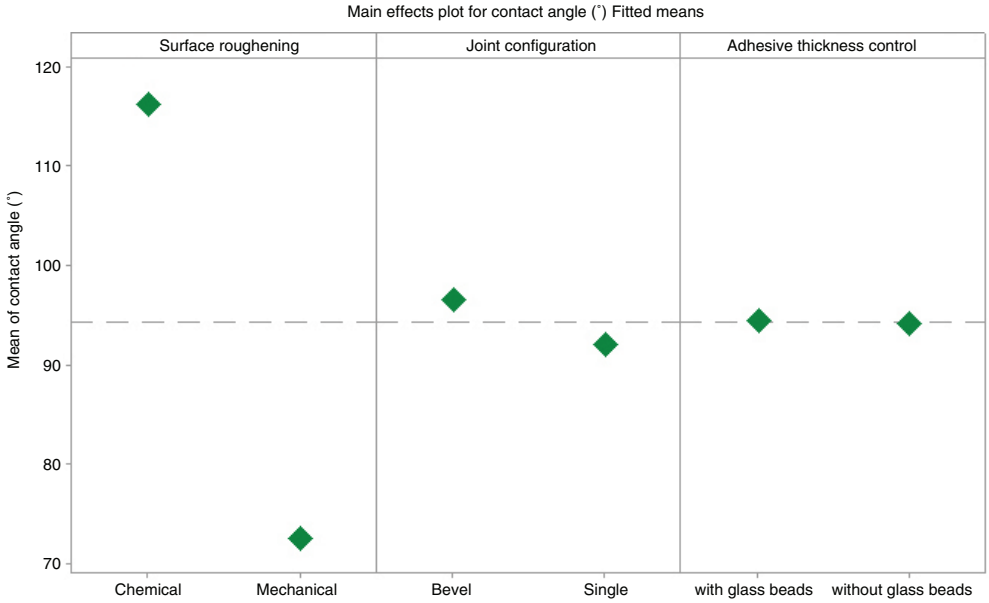

FIGURE 8. Pareto chart for the variables studied in the experimental contact angle.

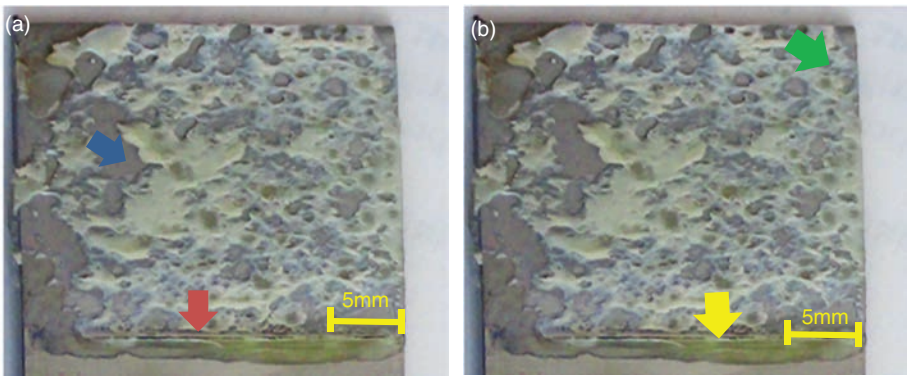

FIGURE 9. Optical images of the surface facture for: a) Specimen number 11 surface failure and b) specimen number 4.

of the failure surface of specimen 11 where a dimple-like morphology is observed. This dimple pattern, that follows the main stress path indicated by the yellow arrow, is appreciated in detail in Fig. 10b. The contrast observed in both micrographs do not show evidence of rust, dirt or another possible source of contamination.

On the other hand, the micrograph showed in Fig. 10c, is a magnification of the defect pointed out by the blue arrow on Fig. 9a (specimen 11). Adherent surface finishing of chemical roughening can easily be identified (note the uniformly distributed lined pattern). The contrast in this image indicates a lack of adherence between adhesive and adherent. At higher magnifications (Fig. 10d), the image reveals that the wetting was not good enough to penetrate into the surface valleys, since the morphology observed suggest that the adhesive was deformed following the shear load application to the specimen (see red arrow Fig. 10d). Additionally, in the image there was no found evidence of contamination that could properly affect the adhesion. This was confirmed by the EDS analysis (inset in Fig. 10c), since the chemical composition related to some traces of oils or dirt was not detected. In the case of sample number 4 (Fig. 10e), shows that the fracture has a pattern similar to the observed in the sample 11 (see Fig. 9b), suggesting an overload-like failure. Finally, from Fig. 10f, it is possible to identify that the defect, which initially was believed as adhesive failure, actually is a lack of filling of adhesive into the joint.

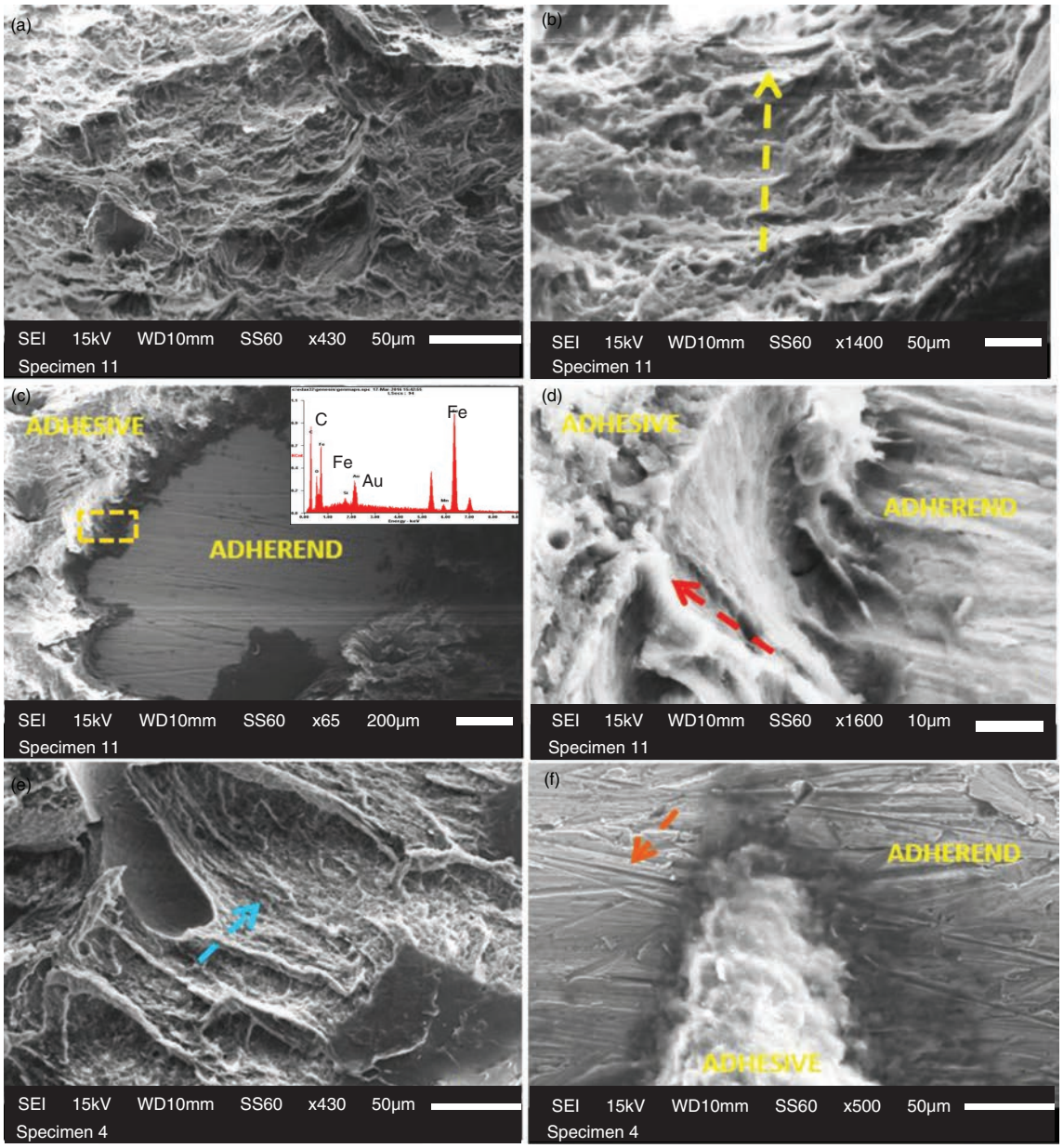

FIGURE 10. a) Micrograph at 430X of sample 11, b) Micrograph at 1400X of sample 11, c) Micrograph at 65X of adhesion failure of sample 11, d) Micrograph at 1600X of sample 12, e) Micrograph at 430X of specimen 4 and f) Micrograph at 500X of lack of filling in sample 4.

4. DISCUSSION

From the results described before we can confirm that the contact angle measurements can be used to map surfaces, in terms of hydrophility, presence of low surface tension components or contaminants, variations in composition or effectiveness of a surface treatment (Bauknecht *et al.*, 2015). The tangent to the projection of the liquid/vapor interface at the triple line is estimated and the angles measured relative to the flat projection of the possibly rough solid surface (Shanahan and Possart, 2011). Contact angle experiments reveals that significant differences do exist between surface finishing methods. The mechanical roughen has lower contact angles against the chemical one, yielding the highest wettability. These results are in agreement with those contact angle experiments previously reported in the available literature (Petrie, 2007; Shanahan and Possart, 2011). According to Petrie, surface roughening can produce contact angles lesser than 90°, improving joint

strength but the opposite occurs with untreated polyethylene (Petrie, 2007). This means that the wettability and strength could depend of the material. According to (Kubiak *et al.*, 2011a) contact angles depend directly on the material and surface roughness. In their paper Kubiak *et al.* (2009) reported titanium samples in which is observed that by increasing the roughness, the contact angle diminishes, in opposition to what is happening with steel; where, as higher the roughness- higher the wettability. Therefore, this relationship cannot be taken as a rule of thumb, because it depends on the material and its topography. In this sense, our results suggest that for ferritic stainless steel, the chemical roughening yields higher roughness but not a higher wettability and shear strength.

SEM observations allowed us to identify certain differences in surface morphology, as chemically rough specimen present fine evenly distributed marks with some coarse ones. Unlike the chemically rough specimen, the mechanical one, presents randomly distributed coarse marks. It is straightforward to suggest that the mechanically prepared specimen will exhibit the highest roughness. Since the chemical roughening process is performed in a bath, all the fluid surround the specimen, providing marks evenly distributed on the surface. Besides the mechanical roughen process is completely manual and the amount of removed material will depend on the applied force and sand paper quality. Therefore, marks could vary across the surface depending on those factors.

The tridimensional surface analysis, indicates that chemically roughen specimen has large and abrupt difference in peak height distance and some slightly difference in peak to valley depth. This is in agreement to the contour two-dimensional graphs in which an abrupt morphology was observed in the case of chemically rough sample. On the contrary the mechanically rough specimen has smother morphology with less abrupt peaks and valleys. According to Petrie (2007), the mechanical abrasion favors bond strength, its application is fast, low cost and does not require training compared to the use of acid etching in which the bond strength is very good but requires previous training and the cost can be slightly higher (Kubiak *et al.*, 2011b). Work on a simple mechanical mechanism of wetting on rough surfaces; they described it in terms of the barriers formed by the asperity peaks. Also they noted that the most influential roughness parameters relate to the form and distribution of peaks. This could confirm that for higher peaks (rougher surface) the contact line motion can be blocked by the surface asperities. Therefore, a higher apparent contact angle can be observed. As stated on publications made by the Fraunhoffer Institute (Bauknecht *et al.*, 2015) the substrate roughness must not too rough in order to promote good adhesion. Since, the mechanical interlocking theory indicates that the peak high and surface morphology has a strong relationship to shear strength (Pocius, 2012). The results obtained in the surface characterization suggests that the topography of the chemically roughen specimen does not promote the contact line motion because it is abrupt topography and distance between peaks. On the contrary, the mechanically roughen specimen has a surface finishing with groves that seems waterways that can distribute the adhesive easily through them.

In terms of shear strength and failure mode, results of Table 3 suggest that a strong relationship between the analyzed factors and the response exists. The analysis of variance gives an adjusted correlation of 99.26% showing a strong influence for each factor as its P value was lower than 0.05. Although the analysis of variance yielded that all factors (except adhesive thickness control) are significant for the response (shear strength), the Pareto chart allows classifying them in order of importance. The first factor is the Surface Finishing, Joint Configuration and Adhesive Thickness Control, the interaction of Joint Configuration and Adhesive Thickness Control, Surface Finishing and Joint Configuration, Joint Configuration, Surface Finishing and Joint Configuration and finally the thickness control. Additionally, the shear strength values presented some differences (2~10 MPa) with other authors that may be attributed to its chemistry (acrylic content, resin ratio and viscosity) and adherent (width, thickness, material and surface finishing) (Park *et al.*, 2003; Shimizu, *et al.*, 2014).

The post fracture analysis revealed that there are zones in which wetting does not occur and obviously the fracture morphology have its particularities. The specimen number 11 yields a rougher overload failure pattern in comparison to number 4. This could be caused, by zones with lower cohesion forces (not enough adhesion strength) between adherent and adhesive film that promotes an adhesive-cohesive failure. This phenomenon stimulates that the crack propagates through the adhesive film, and when a lower cohesion zone crosses it path changes from the adhesive film to its interface. On the other hand, failure on sample number 4 has a finer failure pattern mainly because the crack initiates and propagates through the adhesive layer. The above could have a close relationship with the joint configuration, mainly because in beveled lap joint stress concentration tends to decrease on the lap edges, whereas in single lap joint, stress concentration is higher (Petrie, 2007), and this could promote different crack growth rates.

Adhesive thickness is also a very important factor because an optimum strength could be achieved when its thickness ranges from 0.06 and 0.12 mm and above 0.12 mm stress distribution is such that the adhesive may easily experience cleavage type

forces (Petrie, 2007). For Ebnesajjad and Landrock (2009) the range for optimal adhesion lies between 0.05–0.25 mm. For both, shims could be used to adjust the thickness control. The glass beads tend to maintain a uniform bond line layer rather than the manual procedure in which differences in thickness and cleavage forces could occur. According to the design of experiments, the thickness control in this case was irrelevant since its values are below 0.3 mm.

5. CONCLUSIONS

In this work, we have studied the influence of several factors (surface roughening, joint configuration and adhesive thickness control) on the shear strength of ferritic stainless steel adherents joined with methyl methacrylate. SEM observations suggest that the mechanical method has a more abrupt morphology (then a higher roughness), the profilometry probes the contrary. The design of experiments (DOE) renders useful information, mainly because their result lead us to conclude that surface finishing is the factor that has the highest influence upon the response (shear strength) and failure mode. Also, we observed that the mixture of the mechanical roughening, with single lap joint altogether with the use of glass beads could produce better results in terms of adhesion and strength. Finally, the best combination of factors for obtaining the highest response is mechanical roughening with 80 sanding; single lap joint and glass beads.

ACKNOWLEDGMENTS

Special thanks to Mr. Gary Johnson, Mr. Edward Kozyol and Mr. Victor García from Adhesives INC Company for their support to this work and provide adhesive for testing. Also special thanks to Dr. Pedro González García, M.Sc. Eneftali Flores and Dr. Miguel Martinez for all its technical advises and facilities. J.D. Mosquera-Artamonov thanks CONACYT for their respective PhD. granted scholarships.

REFERENCES

Adhesive Systems Inc. (2017). Methacrylate Adhesives Bond Similar and Dissimilar Materials. Access 27 Marzo 2018. http://instantca.com/methacrylate/.

ASTM D1002-10 (2010). Standard Test Method for Apparent Shear Strength of Single-Lap-Joint Adhesively Bonded Metal Specimens by Tension Loading (Metal-to-Metal), ASTM International, West Conshohocken, PA, USA.

ASTM D7334−08 (2013). Standard Practice for Surface Wettability of Coatings, Substrates and Pigments by Advancing Contact Angle Measurement. ASTM International, West Conshohocken, PA, USA.

AWS (2007). *Welding Handook. Stainless and Heat Resistant Steels*. Vol. 4, Chapter 5, American Welding Society, USA, pp. 255–318.

Bauknecht, H., Borst, V., Brede, B., GroB, A., Harknensee, A., MeiB, E., Niermann, D., Peshka, P., Theuerkauff, P., Warratz, T. (2015). Adhesive Bonding Technology and Surfaces Training Handbook for European Adhesive Specialist (EAS), Bremen, Germany, p. 32.

Bergström, U., Brottare, I. (1996). *Sheet Steel Handbook, Design Fabrication in high strenght steel*. SSAB Tunnplat AB, pp. 64–90.

Bermejo, R., Oñoro, J., García-Ledesma, R. (2008). Comportamiento a la fatiga de uniones a solape simple con adhesivo epoxi de acero y acero prepintado. *Rev. Metal.* 44 (4), 310–316. https://doi.org/10.3989/revmetalm.2008.v44.i4.120.

Brient, A., Brissot, M., Rouxel, T., Sangleboeuf, J.C. (2011). Influence of Grinding Parameters on Glass Workpieces Surface Finish Using Response Surface Methodology. *J. Manuf. Sci. Eng.* 133 (4), 044501. https://doi.org/10.1115/1.4004317.

Cruz, C., Hiyane, G., Mosquera-Artamonov, J.D., Salgado, J.M. (2014). Optimización del proceso de soldadura GTAW en placas de Ti6Al4V. *Soldag. Insp.* 19 (1), 2–9. https://doi.org/10.1590/S0104-92242014000100002.

Cruz-González, C.E., Gala-Barrón, H.I., Mosquera-Artamonov, J.D., Gámez-Cuatzin, H. (2016). Efecto de la corriente pulsada en el proceso de soldadura GTAW en titanio 6Al4V con y sin metal de aporte. *Rev. Metal.* 52 (3), e071. https://doi.org/10.3989/revmetalm.071.

Dyamenahalli, K., Famili, A., Shandas, R. (2015). *Characterization of shape-memory polymers for biomedical applications. In: Shape Memory Polymers for Biomedical Applications*. Elsevier, pp. 35–63. https://doi.org/10.1016/B978-0-85709-698-2.00003-9.

Ebnesajjad, S., Landrock, A.H. (2009). *Adhesive Applications and Bond Processes. In: Adhesives Technology Handbook*. Chapter 8, Elsevier, pp. 206–234.

Ebnesajjad, S., Landrock, A.H. (2015a). *Introduction and Adhesion Theories. In: Adhesives Technology Handbook*. Chapter 1, Elservier, pp. 1–18. https://doi.org/10.1016/B978-0-323-35595-7.00001-2.

Ebnesajjad, S., Landrock, A.H. (2015b). *Material Surface Preparation Techniques. In: Adhesives Technology Handbook*. Chapter 3, Elsevier, pp. 35–66. https://doi.org/10.1016/B978-0-323-35595-7.00003-6.

Feng, C.-X., Kusiak, A. (2000). Robust Tolerance Synthesis With the Design of Experiments Approach. *J. Manuf. Sci. Eng.* 122 (3), 520–528. https://doi.org/10.1115/1.1285860.

Jin, J., Shi, J. (2000). Diagnostic Feature Extraction From Stamping Tonnage Signals Based on Design of Experiments. *J. Manuf. Sci. Eng.* 122 (2), 360–369. https://doi.org/10.1115/1.538926.

Karachalios, E.F., Adams, R.D., da Silva, F.M. (2013). Single lap joints loaded in tension with ductile steel adherends. *Int. J. Adhes. Adhes.* 43, 96–108. https://doi.org/10.1016/j.ijadhadh.2013.01.017.

Kreibich, U.T., Marcantonio, A.F. (1987). New Developments in Structural Adhesives for the Automotive Industry. *J. Adhesion* 22 (2), 153–165. https://doi.org/10.1080/00218468708074998.

Kubiak, K.J., Mathia, T.G., Wilson, M.C. (2009). Methology for metrology of wettability versus roughness of engineering surfaces. Proceeding of 14th International Congress of Metrology, Paris.

Kubiak, K.J., Wilson, M.C., Mathia, T.G., Carval, P. (2011a). Wettability versus roughness of engineering surfaces. *Wear* 271 (3–4), 523–528. https://doi.org/10.1016/j.wear.2010.03.029.

Kubiak, K.J., Wilson, M.C., Mathia, T., Carras, S. (2011b). Dynamics of contact line motion during the wetting of rough surfaces and correlation with topographical surface parameters. *Scanning* 33 (5), 370–377. https://doi.org/10.1002/sca.20289.

Lanzotti, A., Martorelli, M., Staiano, G. (2015). Understanding Process Parameter Effects of RepRap Open-Source Three-Dimensional Printers Through a Design of Experiments Approach. *J. Manuf. Sci. Eng.* 137 (1), 011017. https://doi.org/10.1115/1.4029045.

Mori, K.I., Bay, N., Fratini, L., Micari, F., Tekkaya, A.E. (2013). Joining by plastic deformation. *CIRP Annals* 62 (2), 673–694. https://doi.org/10.1016/j.cirp.2013.05.004.

Pappas, D.D., Bujanda, A., Yim, J.H., Stawhecker, K., Orlicki, J., Demaree, J., Jensen, R. (2009). Chemical and Topological Study of Atmospheric Pressure Plasma Treated Fibers and Polymer Films. Technical Conference, 52nd, Society of Vacuum Coaters, Santa Clara, CA.

Park, K.D., Kim, J., Yang, S.J., Yao, A., Park, J.B. (2003). Preliminary study of interfacial shear strength between PMMA precoated UHMWPE acetabular cup and PMMA bone cement. *J. Biomed. Mater. Res. B* 15 (65), 272–279. https://doi.org/10.1002/jbm.b.10006.

Petrie, E.M. (2007). *Theories of Adhesion. In: Handbook of Adhesives and Sealants*. Chapter 2, New York, USA, Mac Graw-Hill, pp. 39–57.

Pocius, A.V. (2012). *The Relationship of Surface Science and Adhesion Science*. *In: Adhesion and Adhesives Technology*. Chapter 6, Hanser Publishers, pp. 145–179.

Shanahan, M., Possart, W. (2011). *Wetting of Solids. In: Handbook of Adhesion Technology*. Adams, R.D., da Silva, L., Oschner, A. (Eds), Springer, Berlin, Heidelberg, pp. 65–91.

Shimizu, K., Malmos, K., Hjarbæk, A., Uttrup, S., Daasberj, K., Hinge, M. (2014). Improved Adhesion Between PMMA and Stainless Steel Modified with PMMA Brushes. *ACS Appl. Mater. Inter.* 6 (23), 21308–21315. https://doi.org/10.1021/am5062823.